Journal of Biomechanics 151 (2023) 111517

Contents lists available at ScienceDirect

Journal of Biomechanics

journal homepage: www.elsevier.com/locate/jbiomech

A statistical model to predict the occurrence of blunt impact injuries on the human hand-arm system

R. Behrens [a,*], G. Pliske [b], S. Piatek [b], F. Walcher [b], N. Elkmann [a]

[a] Fraunhofer IFF, Sandtorstr. 22, 39106 Magdeburg, Germany

[b] Department of Trauma Surgery, Otto von Guericke University, Leipziger Str. 44, 39120 Magdeburg, Germany

ARTICLE INFO

Keywords:
Injury onset
Pain onset
Biomechanical limits
Human subject study
Cobots
Collaborative robots

ABSTRACT

Biomechanical limits based on pain thresholds ensure safety in workplaces where humans and cobots (collaborative robots) work together. Standardization bodies' decision to rely on pain thresholds stems from the assumption that such limits inherently protect humans from injury. This assumption has never been verified, though. This article reports on a study with 22 human subjects in which we studied injury onset in four locations of the hand-arm system using an impact pendulum. During the tests, the impact intensity was slowly increased over several weeks until a blunt injury, i.e., bruising or swelling, appeared in the body locations under load. A statistical model, which calculates injury limits for a given percentile, was developed based on the data. A comparison of our injury limits for the 25th percentile with existing pain limits confirms that pain limits provide suitable protection against impact injuries, albeit not for all body locations.

1. Introduction

Cobots (collaborative robots) are ushering a new form of industrial workplace that improves work conditions (Hentout et al., 2019). Their human-friendly design and sophisticated sensors make them safe to operate right next to humans (Villani et al., 2018; Krüger et al., 2009). Biomechanical limits specify the maximum forces and peak pressures for different body locations, which cobots may not exceed if they collide with humans. The force and pressure limits currently in use for cobots are reflective of pain thresholds that were ascertained experimentally in human subject studies (Park et al., 2019; Melia et al., 2019; Behrens et al., 2022). Their reliability to protect humans from injuries is questionable since humans' ability to sense pain is strongly subject to emotional factors (Behrens and Elkmann, 2021). Pain limits can be deemed injury-preventive when the findings of objective observations indicate that they are below the threshold of injury onset.

We define injury onset as the threshold between pain and blunt trauma manifested by bruising or swelling without any laceration, abrasion, or fracture. External forces cause bruising when blood vessels are deformed beyond their recoverable limits at which they begin to rupture (Silver et al., 2003; Viano et al., 1989; Kieser et al., 2012; Di Maio and Di Maio, 2001). Gravitational forces transport leaked blood to the epidermis where it causes the typical discoloration (Di Maio and Di Maio, 2001). Swelling caused by fibrin leaking into tissue is often a side effect (Szczesny et al., 2001).

The shape and kinetic energy of the object that collides with a human body dictate the injury severity. Although kinetic energy plays an important role, early research has shown that the rate and magnitude of the contact force correlate best with the degree of tissue damage (Hodgson et al., 1964; Gadd et al., 1968). This sensitivity is attributable to the viscous-elasticity of soft tissue (Viano et al., 1989; Viano and Lau, 1988). The anatomical variety of the human body is another factor that causes tolerance levels to differ (Sugiura et al., 2019; Raymond et al., 2009; Etheridge et al., 2005; Smalls et al., 2006). Demographic parameters, such as age (Pintar et al., 1998b; Zhou et al., 1996; Kent and Patrie, 2005; Nyquist, 1986; Haut, 2002; Bader and Bowker, 1983) and gender (Cesari et al., 1980; Gadd et al., 1968; Pintar et al., 1998a.; Viano et al., 1989; Bader and Bowker, 1983), also influence human injury tolerance.

Only a few trauma studies have explored the mechanisms of slight blunt injuries, such as bruising, albeit usually using porcine tissue or pigs as subjects (Barington and Jensen, 2016; Fujikawa et al., 2017; Sugiura et al., 2019; Shen et al., 2008; Sharkey et al., 2012; Mao et al., 2015). Reliable limits for humans can only be expected from human subject studies (Crandall et al., 2011; King et al., 1995; Payne et al., 2013), though, such as those conducted by Desmoulin and Anderson (2011) and Black et al. (2019). Given the small subject groups and improper testing systems, the data from both studies are virtually

* Corresponding author.
E-mail address: roland.behrens@iff.fraunhofer.de (R. Behrens).
URL: https://www.iff.fraunhofer.de/rs (R. Behrens).

https://doi.org/10.1016/j.jbiomech.2023.111517
Accepted 22 February 2023
Available online 24 February 2023

unusable for assessing the reliability of the pain limits currently used for cobots.

In this article, we present an impact study in which we experimentally determined injury onset thresholds of four body locations in the human hand-arm system. Our aim was to develop a parametric model from censored observations obtained from our experiments, which reproduces the observations' statistical distribution. The model we designed enabled us to calculate the desired injury onset limits, which we then compared with the pain limits currently used for cobots. The comparison indicates that the pain limits reliably protect humans from impact injuries.

2. Methods and materials

In our study, we followed the approach of acquiring data in experimental impact tests with humans. We slowly increased the impact intensity over a long period until signs of bruising or swelling appeared on the body locations tested. The ethics committee of Otto von Guericke University (Magdeburg, Germany) reviewed and approved the study (reference number 47/13).

2.1. Human subjects

All in all, 24 subjects (12 females and 12 males) participated in the study. None of them had preexisting conditions that could have caused complications or biased the results. Table 1 presents an overview of the subjects' body parameters and the groups to which they were assigned. Two female subjects from G1 and G3 quit the study before the experiments had ended. Their data were discarded.

Table 1
Body parameters of the subjects of the study.

Group	Females	Males	Both	Age (y)	Height (m)	Weight (kg)
G1	7	8	15	39.3±14.3	1.75±0.07	70.0±8.6
G2	2	2	4	47.8±21.6	1.81±0.11	81.8±22.2
G3	1	2	3	49.0±14.9	1.79±0.06	77.7±8.4

2.2. Relevant variables

The variable used most frequently to set biomechanical limits is *maximum force* $\hat{F}_C$ (Yamada et al., 1996; Saito and Ikeda, 2005; Mewes and Mauser, 2003; Behrens and Elkmann, 2014), i.e., the highest magnitude of three-dimensional impact force $\mathbf{f}_C \in \mathbb{R}^{3\times1}$ during contact time τ

$$\hat{F}_C = \max_{0\leq t\leq\tau} \|\mathbf{f}_C(t)\| \quad . \tag{1}$$

Since force limits do not include any information about the contact surface $\partial\mathbb{X}_H$, they are only valid in conjunction with a specific contact surface $\hat{F}_C := \hat{F}_C(\partial\mathbb{X}_H)$. Limits based on normal stress, such as *peak pressure*, reflect the highest force concentration within the contact area and consequently include information on $\partial\mathbb{X}_H$. The peak pressure $\hat{\psi}_C$ coincides with the highest magnitude of the time-dependent stress field $\mathbf{\Psi}_C(\mathbf{x},t)$ created by the impact at position $\mathbf{x} \in \mathbb{R}^{3\times1}$ on $\partial\mathbb{X}_H$

$$\hat{\psi}_C = \max_{0\leq t\leq\tau,\mathbf{x}} \mathbf{\Psi}_C(\mathbf{x},t) \quad . \tag{2}$$

The relationship between $\mathbf{f}_C$ and $\mathbf{\Psi}_C(\mathbf{x},t)$ is established by

$$\mathbf{f}_C = \int_{\partial\mathbb{X}_H} \mathbf{\Psi}_C(\mathbf{x},t)dA \quad , \tag{3}$$

where dA denotes an infinitesimal element on $\partial\mathbb{X}_H$ at $\mathbf{x}$. The *maximum energy density* is another variable that has been used in the past to set biomechanical limits (Povse et al., 2011; Cardany et al., 1976; Hallowell et al., 2017). It is derived from the energy density e_C, i.e., the concentration of impact energy within the contact area

$$e_C = \int_0^{x_d(t)} \mathbf{\Psi}_C(\mathbf{x},t)dx_d \quad , \tag{4}$$

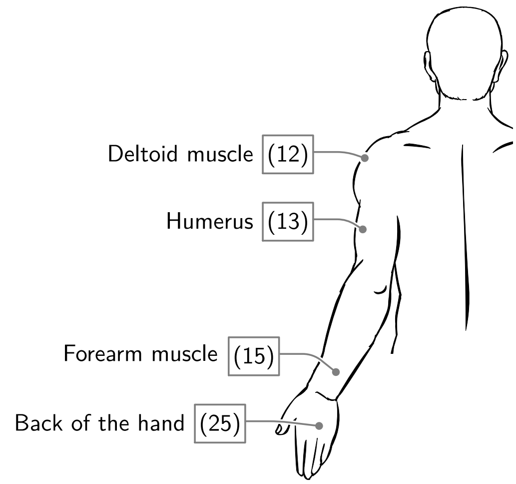

Fig. 1. Body locations on the arm and non-dominant hand tested in the study. The identifiers are the same as the ones used in ISO/TS 15066. Anatomical landmarks were used to localize the body locations (see the Appendix).

where x_d is the deformation of the body location. The maximum energy density $\hat{e}_C$ is yielded by

$$\hat{e}_C = \max_{\mathbf{x},t} e_C(\mathbf{x},t) \quad . \tag{5}$$

2.3. Experimental setup

2.3.1. Conditions

The findings presented by Behrens et al. (2022) indicate that the human arm and hand, especially locations other than fingers, joints and the like with underlying nerve tracts, have a high tolerance to impact loads. Studying the hand-arm system first is expedient since human arms and hands are the limbs most frequently exposed to robot collisions. We selected four body locations in different regions of the hand-arm system (see Fig. 1). This constituted the first experimental condition. These body locations are a subset of the body locations for which (ISO/TS 15066, 2016) specifies pain limits for use in robotics. Distinct anatomical landmarks enabled us to precisely localize the contact points to be tested (see the Appendix).

The surface of a colliding object significantly influences an impact's potential to cause injury. The shapes of the contact bodies used in the impact tests are consequently the second experimental condition. We were only able to find one contact body, called F-Q10, in the literature, which had been used in other studies (Behrens et al., 2022; Park et al., 2019; Melia et al., 2019). It is an aluminum cuboid, each edge of which measures 14 mm in length. Its edges are rounded to a radius of 2 mm (see Fig. 2). The other contact bodies C-R5 and C-R40 made of polyoxymethylene reproduce typical shapes found on robot surfaces. C-R5 resembles a wedge with a vertical angle of 30° and a width of 80 mm. The sharp edge that points toward the subject is rounded to a radius of 5 mm. C-R40 has a convex contact surface with a radius of 40 mm, a height of 45 mm and a width of 51 mm. Table 2 indicates which contact body was used for which subject group.

Maximum impact force can be estimated using the following simplified model (Hodgson et al., 1965)

$$\hat{F}_C \approx \sqrt{m_I c_H} v_I \quad , \tag{6}$$

where m_I is the impact mass, v_I the impact velocity and c_H the elasticity of the body location under load. Both parameters are consequently additional experimental conditions. Given Eq. (3), both parameters not only influence $\hat{F}_C$ but also $\hat{\psi}_C$ and $\hat{e}_C$. We tested each human subject with three different impact masses $m_I \in \{5.7\,\text{kg}, 10.7\,\text{kg}, 16.0\,\text{kg}\}$. The impact velocity v_I was gradually increased until the impact caused swelling or bruising.

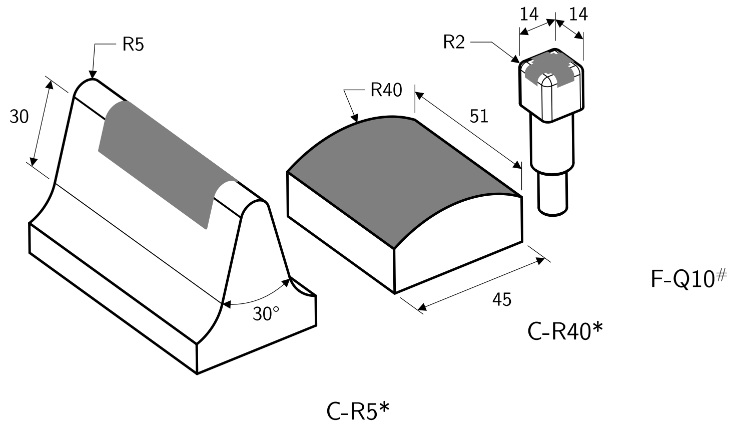

Fig. 2. Contact bodies used in the impact experiments. A pressure-sensitive film (gray area) was affixed to the contact body's surface in every test. C-R5 and C-R40 are made of polyoxymethylene and F-Q10 is made of aluminum.

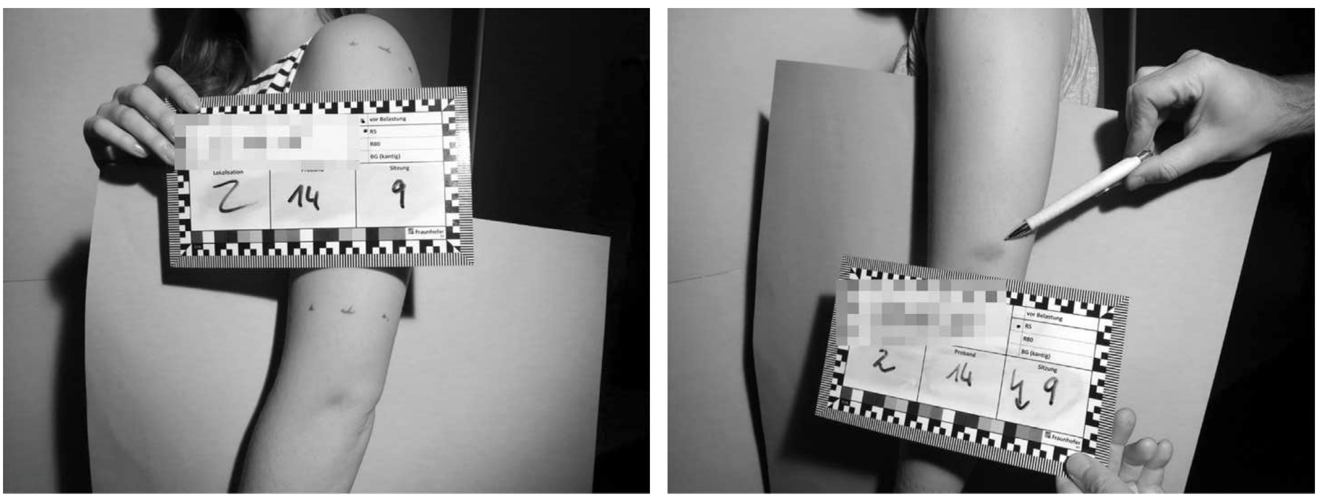

Fig. 3. Picture of body location (13) humerus taken before an impact test with C-R5 (left). One week later, discoloration had become visible on the skin, indicating bruising (right). This was treated as a positive observation.

Table 2
Distribution of the individual test outcomes where N_L is the number of left-censored, N_I the number of interval-censored and N_R the number of right-censored observations. Variable N is the total number of tests that caused swelling or bruising (i.e., true positive observations).

Subject group	Body part	N_L	N_I	N_R	N
G1 (C-R5)	(12) Deltoid m.	0	5	32	37
	(13) Humerus	8	22	15	45
	(15) Forearm m.	7	18	17	42
	(25) Back of the hand	7	18	20	45
G2 (F-Q10)	(12) Deltoid m.	0	2	6	8
	(13) Humerus	0	7	4	11
	(15) Forearm m.	0	8	3	11
	(25) Back of the hand	0	6	6	12
G3 (C-R40)	(12) Deltoid m.	0	0	4	4
	(13) Humerus	0	2	3	5
	(15) Forearm m.	0	1	5	6
	(25) Back of the hand	0	2	7	9

2.3.2. Impact pendulum

In the study, we used the same pendulum as Behrens et al. (2022) to replicate typical load intensities as they occur in robot collisions. It was designed like other pendulums (Dhaliwal et al., 2002; Muggenthaler et al., 2006; Randeberg et al., 2007; Delye et al., 2007; Han et al., 2021) and provided means to vary m_I and v_I in the range of cobots' parameters. The pendulum resembles a four-bar linkage with two parallel bars, each of which measures 0.8 m in length. A deflection mechanism at the rear of the pendulum enabled us to increase the impact velocity v_I in steps of 0.05 m/s up to 1.25 m/s. Additional weights can easily be attached to the pendulum body, making it possible to vary the impact mass m_I between 1.9 kg and 20 kg. Each of the aforementioned contact bodies (see Fig. 2) can be mounted on the piezoelectric load cell (KISTLER 9327C with a range of ±1 kN and a maximum error of 1.61 %) located at the front of the pendulum body. The load cell records the force in all three dimensions at 10 kHz and 16 bit, as in other studies (Dhaliwal et al., 2002; Povse et al., 2011). Pressure sensitive films were affixed to the surface of each contact body (TekScan I-Scan 5120 and 4205, range of 1.2 kN/cm^2 and maximum error of 10 %). Each of the films sample pressure at 1.24 kHz (film 4205) and 2.07 kHz (film 5120) with a resolution of 8 bit.

2.3.3. Test procedure

The experiments were conducted in weekly sessions during which the subjects' body locations were subjected to testing just once a week. This provided enough time for subcutaneous bleeding to appear on the skin. The body locations were visually examined and palpated at the start of each session to ensure that they did not display signs of bruising or increased tenderness. In the event a bruise was visible, the previous session's outcome was counted as a true-positive observation (i.e., blunt injury). All uninjured body locations were marked and photographed afterward (see Fig. 3).

A subject's arm was positioned in front of the pendulum to ensure that the impact force acted perpendicular to each body location.

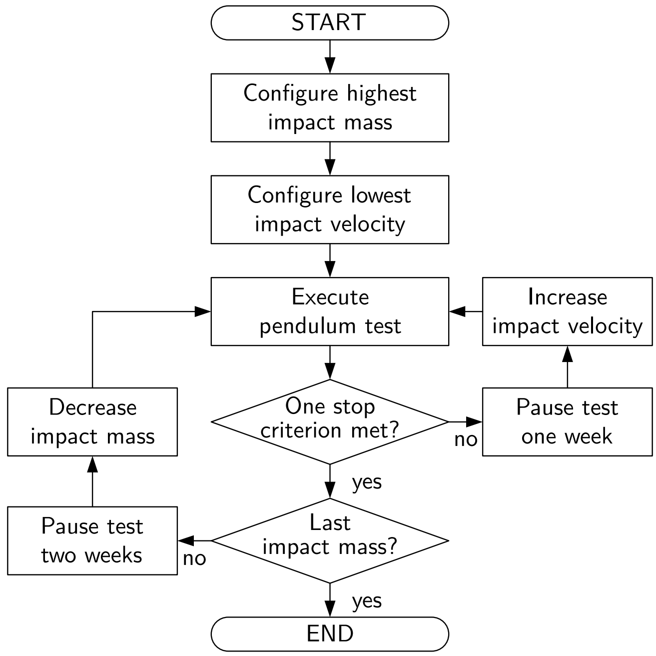

Fig. 4. Iterative procedure applied to vary impact mass and impact velocity in a minimum number of tests per subject.

Vacuum cushions and straps secured the arm's position. Subjects wore eye masks and headphones played with nature sounds during impact tests to retain the element of surprise. Once everything was properly arranged, the experimenter released the pendulum, which then struck the body location at the desired impact velocity.

Immediately after being struck, the subject was asked to rate the intensity of the pain felt by drawing a line on a printed 100 mm visual analog scale (VAS). The VAS comprises eleven segments ranging from "no pain" to "unbearable pain". A line measuring ≥50 mm or longer indicates that a subject's pain tolerance threshold (PTT) and thus the range of tolerable pain was exceeded (Lacourt et al., 2012). Ethical boundaries made the exceedance of the PTT the second stopping criterion.

All body locations were visually reexamined for signs of swelling after the tests. The appearance of swelling constituted the first stopping criterion and meant to discontinue the tests on the injured body location for at least two weeks. This period roughly corresponds to the healing time of a bruise (Black et al., 2019). To minimize the total number of tests per subject, we always started the first session with the highest impact mass 16.0 kg and switched to the next lower mass once one of the stopping criteria had been met (see Fig. 4). Since this procedure also reduces $\hat{F}_C$ (and all other relevant variables), the force from the preceding test could not be exceeded (see (6)). This enabled us to increase the last velocity set rather than having to restart with the lowest velocity adjustable.

2.3.4. Signal processing

A phase-zero and fourth-order Butterworth low-pass filter with a channel frequency class (CFC) of 100 was applied to reduce the noise in the time-resolved force and pressure signals (J211-1, S., 2014). Once the force signals had been filtered, we applied the following scaling factor to eliminate the deviation of the force measured $\mathbf{f}_M$ from the actual contact force $\mathbf{f}_C$ caused by the position and inertia of the contact bodies (Nahum et al., 1972; Stalnaker and Melvin, 1976)

$$\mathbf{f}_C = \left(1 + \frac{m_I}{m_B}\right)\mathbf{f}_M \quad , \tag{7}$$

where m_B is the pendulum body mass and m_I is the mass of the contact body attached to the load cell. Once the signals had been processed, the maximum contact force $\hat{F}_C$, peak pressure $\hat{\psi}_C$ and energy density $\hat{e}_C$ were determined and calculated, as described in Section 2.2. The signals recorded by the pressure films were additionally processed with the same Gaussian filter and interpolation technique employed in Behrens et al. (2022).

2.4. Data analysis

Approaching injury onset with velocity steps of 0.05 m/s inevitably produced censored observations, i.e., the true but unknown observation y_i lies within the interval $(L_i, R_i]$ spanned by the observations from the penultimate and final tests. An observation is denoted as interval-censored when $L_i > 0$ and $R_i < \infty$. Otherwise, y_i is denoted as left-censored $L_i = 0$ when the first test with the lowest possible impact velocity already caused an injury (i.e., limit of detection) and right-censored $R_i \to \infty$ when the last test with the highest possible impact velocity did not cause any injury (i.e., limit of quantification). To calculate limits from the samples, we modeled the observations' distribution using a cumulative distribution function (CDF) that expresses injury probability p as a function of load intensity y_p as follows

$$\mathcal{F}(y_p) = p \quad . \tag{8}$$

The CDF can be parametric ($\mathcal{F}(y)$; theoretical CDF) or nonparametric ($\mathcal{F}_n(y)$; empirical CDF).

Given the second stopping criterion (exceedance of a subject's PTT), we had to assume that a significant number of samples would contain more right-censored than left- and interval-censored observations. These samples are treated as *unbalanced* samples, all others as *balanced* samples. Each sample type required a different methodology for estimating $\mathcal{F}_n(y)$ and the parameter vector $\mathbf{p}$ for $\mathcal{F}(y)$.

Method for balanced samples. The Turnbull algorithm was specifically designed to estimate $\mathcal{F}_n(y)$ from samples with censored observations (Lindsey and Ryan, 1998) and is therefore used here (and designated "method 1" or M1). Since the algorithm cannot estimate probabilities for load intensities above the maximum B_{max} of all observations in a sample with

$$B_{max} = \max_i \{L_i, R_i\} \quad , \tag{9}$$

it will most likely truncate the curve that plots $\mathcal{F}_n(y)$. The curve must therefore be modeled with $\mathcal{F}(y)$ in order to calculate probabilities for

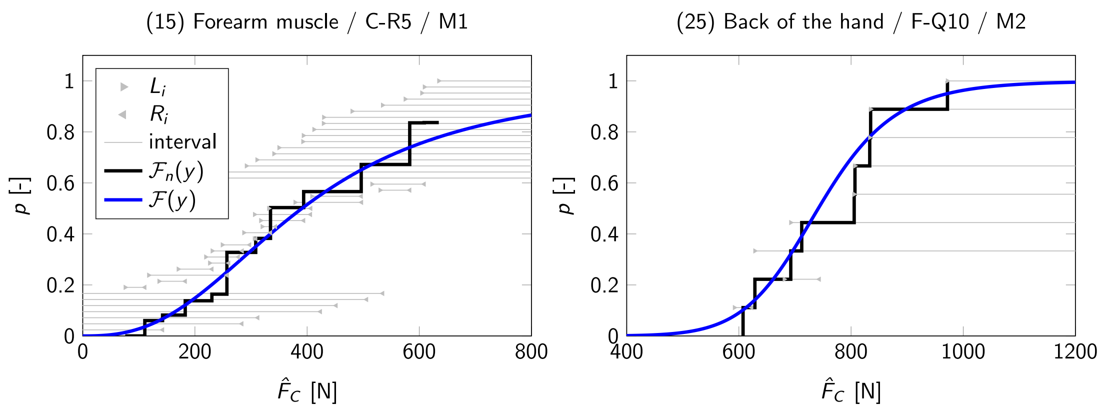

Fig. 5. Nonparametric CDF $\mathcal{F}_n(y)$ and parametric CDF $\mathcal{F}(y)$ estimated from samples measured in tests with C-R5 on (15) forearm muscle and F-Q10 on (25) back of the hand using method 1 (M1) and method 2 (M2).

Table 3
Limit for the 25th percentile of the injury onset threshold based on the maximum contact force $\hat{F}_C$ in [N], peak pressure $\hat{\psi}_C$ in [N/cm^2] and maximum energy density $\hat{e}_C$ in [J/cm^2]. The confidence interval $[y^L, y^U]$ corresponds to a confidence level of 95 %.

Group	Body part	F_{25}	$[F_{25}^L, F_{25}^U]$	ψ_{25}	$[\psi_{25}^L, \psi_{25}^U]$	e_{25}	$[e_{25}^L, e_{25}^U]$
G1	(12) Deltoid m.	372	[253, 723]	150	[122, 187]	1.91	[1.23, 2.71]
(C-R5)	(13) Humerus	115	[66, 181]	145	[95, 222]	0.52	[0.32, 0.95]
	(15) Forearm m.	256	[174, 334]	348	[250, 514]	0.71	[0.34, 1.08]
	(25) Back of the hand	303	[224, 387]	1048	[676, 1414]	2.31	[1.22, 4.31]
G2	(12) Deltoid m.	211	[170, 264]	236	[193, 289]	5.98	[4.15, 8.00]
(F-Q10)	(13) Humerus	114	[38, 210]	191	[76, 317]	0.48	[0.16, 1.48]
	(15) Forearm m.	220	[149, 320]	235	[188, 444]	0.85	[0.57, 1.92]
	(25) Back of the hand	249	[217, 287]	1038	[974, 1096]	3.14	[2.88, 3.55]
G3	(12) Deltoid m.	341	[330, 382]	118	[110, 136]	2.55	[1.75, 3.39]
(C-R40)	(13) Humerus	642	[571, 770]	138	[130, 169]	1.03	[0.86, 1.39]
	(15) Forearm m.	900	[846, 966]	153	[140, 190]	1.07	[0.97, 1.37]
	(25) Back of the hand	692	[614, 781]	526	[483, 601]	2.53	[2.08, 3.38]

$y > B_{max}$ with (8). An estimate of $\mathbf{p}$ can be obtained using maximum likelihood estimation (MLE) and the likelihood function for differently censored observations, as developed by Delignette-Muller and Dutang (2015).

Method for unbalanced samples. We synthesized observations y_i using midpoint imputation to estimate the nonparametric and parametric CDF for unbalanced samples. This method (designated “method 2” or M2) assumes that $\check{y}_i$ lies in the center of $(L_i, R_i]$ (Sun, 2006). Right-censored observations must be treated differently since they do not have a finite upper boundary $R_i \to \infty$. As a workaround, y_i can be underestimated by setting it to L_i. Left-censored observations with $L_i \to -\infty$ must be treated differently too. Assuming that an impact with zero force cannot cause injury results in $L_i = 0$ and an estimate of y_i in the center of $(0, R_i]$. The following expression summarizes all the cases

$$\check{y}_i = \begin{cases} \frac{1}{2} R_i & L_i = 0 \\ L_i & R_i \to \infty \\ \frac{1}{2}(L_i + R_i) & \text{otherwise} \end{cases} . \tag{10}$$

(10) renders all observations scalar values and makes it possible to estimate $\mathcal{F}_n(y)$ with the accumulated relative frequencies and $\mathcal{F}(y)$ with the MLE based on the standard likelihood function.

3. Results

We conducted over 1000 impact tests, which ultimately produced a surprisingly small number of clearly visible bruises or swollen areas (i.e., true positive observations). Table 2 breaks down the number of differently censored data obtained from the load tests. Observations from tests in which subjects had felt pain in the range of their pain tolerance threshold or beyond were not treated as right-censored and, thus, discarded. The decision was made since a right-censored observation is defined as a result from a test with maximum impact velocity and without relevant consequences (i.e., limit of detection). As we expected before the experiments, the number of right-censored observations in some samples, e.g., from tests with the large contact body C-R40, exceeds the number of interval- or left censored observations. The observations in these samples had to be modeled using the method for unbalanced samples (method 2; see Section 2.4).

3.1. Data distribution

To express $\mathcal{F}(y)$, we analyzed the log-normal, Weibull, and log-logistic CDFs, which are normally best suited for modeling injury probabilities in trauma biomechanics (Kent et al., 2004). An Anderson–Darling test with all samples revealed that the log-logistic CDF matches the data best. The log-logistic CDF is obtained from

$$\mathcal{F}(y) = \left\{ 1 + \left(\frac{y}{y_0} \right)^{-a} \right\}^{-1} , \tag{11}$$

where y_0 is the scale and a the shape parameter. The graphs in Fig. 5 plot $\mathcal{F}_n(y)$ and $\mathcal{F}(y)$ on the log-logistic model for tests with C-R5 on the (15) forearm muscle (left) and tests with F-Q10 on the (25) back of the hand (right). Table 4 lists the parameters estimated from all balanced and unbalanced samples for $\hat{F}_C$, $\hat{\psi}_C$, and $\hat{e}_C$. The coefficients of determination R^2 also listed in Table 4 confirm that most parameters yield a good fit of the observations' distribution ($\min R^2 = 0.688$, $\max R^2 = 0.981$, and $\bar{R}^2 = 0.884$).

3.2. Injury onset limits

The pain limits currently used for cobots reflect the 75th percentile (P75) of human workers' pain onset thresholds. Behrens and Elkmann

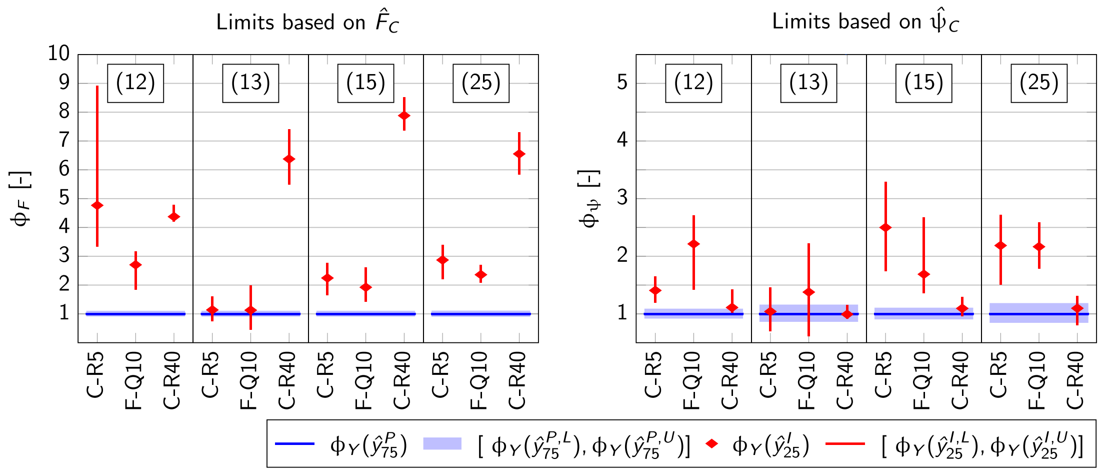

Fig. 6. Relative comparison of pain limits (75th percentile) from Behrens et al. (2022) with injury limits (25th percentile) from this article. The distances of the red diamonds from the blue line indicate the relative differences between pain and injury limits. The blue region is the normalized CI of the pain limits. The red whiskers are the normalized CI of the injury limits. (For interpretation of the references to color in this figure legend, the reader is referred to the web version of this article.)

Table 4
Estimated shape parameters $\hat{y}_0$ and scale parameters $\hat{a}$ for all samples. The coefficients of determination R^2 reflect the model's goodness of fit. The last column specifies the method used to estimate the parameter (M1 for balanced samples and M2 for unbalanced samples).

Group	Body part	$\hat{F}_C$			$\hat{\psi}_C$			$\hat{e}_C$			M
		$\hat{y}_0$	$\hat{a}$	R^2	$\hat{y}_0$	$\hat{a}$	R^2	$\hat{y}_0$	$\hat{a}$	R^2	
G1	(12) Deltoid m.	570	2.57	0.688	197	4.05	0.981	2.90	2.62	0.965	1
(C-R5)	(13) Humerus	231	1.56	0.960	299	1.52	0.922	1.33	1.18	0.868	1
	(15) Forearm m.	391	2.61	0.967	606	1.98	0.964	1.46	1.53	0.884	1
	(25) Back of the hand	424	3.29	0.908	1602	2.59	0.858	5.12	1.38	0.787	1
G2	(12) Deltoid m.	243	7.78	0.970	283	6.10	0.962	7.55	4.74	0.955	2
(F-Q10)	(13) Humerus	208	1.82	0.813	313	2.24	0.856	1.13	1.29	0.834	1
	(15) Forearm m.	293	3.82	0.738	348	2.81	0.715	1.48	1.98	0.708	1
	(25) Back of the hand	277	10.29	0.927	1231	6.45	0.817	3.83	5.51	0.814	1
G3	(12) Deltoid m.	358	22.28	0.857	132	10.36	0.794	3.07	5.87	0.906	2
(C-R40)	(13) Humerus	709	11.10	0.947	150	12.63	0.875	1.22	6.18	0.956	2
	(15) Forearm m.	946	22.33	0.950	180	6.72	0.909	1.33	5.04	0.904	2
	(25) Back of the hand	761	11.72	0.940	618	6.84	0.946	3.14	5.06	0.979	2

(2021) recommend adding new limits for the 25th percentile (P25) of thresholds for blunt injury onset to the current pain limits. We used the parameters listed in Table 4 and the inversion of (8) to calculate the P25 limits for blunt injury onset and their confidence intervals (CI; confidence level of 95 %) presented in Table 3. Since our data include repeated measures, cluster bootstrapping was used to incorporate the inter-subject variance in the estimation of each sample's CI. A similar procedure was presented by Bellamy et al. (2004). In our case, a cluster includes all observations related to one subject.

To compare our P25 injury limits $\hat{y}^I_{25}$ with currently available P75 pain limits $\hat{y}^P_{75}$, we treat $\hat{y}^P_{75}$ as the reference based on which $\hat{y}^I_{25}$ and their CIs $[\hat{y}^{I,L}_{25}, \hat{y}^{I,U}_{25}]$ are normalized as follows

$$\phi_Y(y) = \frac{y}{\hat{y}^P_{75}} \quad . \tag{12}$$

Fig. 6 plots the relative differences between both limit types based on maximum force $Y \hat{=} \hat{F}_C$ (left graph) and peak pressure $Y \hat{=} \hat{\psi}_C$ (right graph). A graph for $\hat{e}_C$ (energy density) could not be plotted since it has not yet been used to specify pain limits. The blue bottom lines denote the position of $\phi_Y(\hat{y}^P_{75}) = 1$ in each section. They are enclosed by blue regions signifying the pain limits' normalized CIs $[\phi_Y(\hat{y}^{P,L}_{75}), \phi_Y(\hat{y}^{P,U}_{75})]$. Red diamonds and vertical lines plot the position of the normalized injury limits $\phi_Y(\hat{y}^I_{25})$ and their normalized CIs $[\phi_Y(\hat{y}^{I,L}_{25}), \phi_Y(\hat{y}^{I,U}_{25})]$. Whenever a normalized CI of an injury limit overlaps with a blue region around a bottom line, the related pain limit is probably unable to protect the related body location from injury.

4. Discussion

Little was known about blunt injury onset and its threshold's impact intensities prior to our study. To date, only Desmoulin and Anderson (2011) and Black et al. (2019) have conducted impact experiments with human subjects in which bruising was produced on various body parts. The low number of injury studies with human subjects is most likely attributable to ethical barriers or difficulties protecting study participants from serious injuries (e.g., fractures). We designed a new and ethically acceptable approach to experiments for our study of the onset of blunt impact injuries. The experiments were specifically designed to replicate typical impact loads that act on the human body in collisions with cobots. Protection from serious injuries was primarily ensured by employing a simple pendulum as the testing instrument to slowly approach the injury onset threshold over a long testing period. A stopping criterion related to the subjects' individual pain tolerance threshold additionally ensured that we did not subject participants to unethically high impact loads.

The objective of our study was to calculate limits for a specific percentile of the test population's individual blunt injury thresholds. Following Desmoulin and Anderson (2011) and Kent et al. (2004), we used a log-logistic CDF to model the injury probability as a function of impact intensity. A load-cell and pressure films enabled us to express the impact intensity with three different variables, specifically maximum impact force, pressure and energy density. The ability to calculate force and pressure limits is essential to expanding the current pain limits specified by ISO/TS 15066 (2016). The model parameters listed in Table 4 can be used to calculate limits for any percentile. It is, however, strongly advised to treat all the limits obtained with caution since most of the parameters are based on data from quite small samples (see Table 1). Organizational and budgetary constraints precluded the involvement of more subjects, though. The small sample sizes consequently made it impossible to analyze covariates (e.g., impact mass or gender).

Of course, our test procedure has limitations and potential sources of errors that may affect the quality and validity of our findings. For instance, interrater and intrarater differences cannot be analyzed. Only one experimenter performed the tests throughout the entire study. Moreover, each combination of experimental conditions was only tested once. These circumstances make it difficult to detect systematic errors. We gave priority to developing a detailed study protocol that clearly guides the experimenter through all steps to reduce interrater differences. One potential source of error was the visual examination of the body locations for signs of bruising and/or swelling, which can yield false negative observations. To verify its reliability, we also took blood samples from and body temperatures of all subjects and examined some with magnetic resonance imaging (MRI). We intend to analyze the correlation of the additional data with the results from the visual examination in our next article.

The small and sometimes unbalanced samples notwithstanding, we are confident that our results provide valuable insight into the reliability of pain onset limits, as we intended. As stated in Section 3.2, we deem P75 pain limits injury-preventive when their CIs do not overlap with the CIs of the P25 injury limits listed in Table 3. We used pain limits from our recent article (Behrens et al., 2022) as reference values. In Fig. 6, the overlap for body location (13) in the right-hand graph indicates that the related pain limit based on $\hat{F}_C$ does not provide protection against impact injuries from semi-sharp surfaces. The results from the tests with C-R5 and F-Q10 illustrate this quite clearly. The limits for C-R40 paint a different picture and demonstrate that limits for blunt surfaces ought to be based on $\hat{F}_C$ and data measured with large contact bodies such as C-R40. The overlap for C-R40 in the left-hand graph indicates that injury limits based on $\hat{\psi}_C$ are better suited for semi-sharp contact surfaces, except for body location (13) where we are unable to confirm that P75 pain limits are injury-preventive for blunt or semi-sharp surfaces, as assumed in ISO/TS 15066 (2016).

5. Conclusion and outlook

In this article, we presented an experimental study in which we performed impact tests on four locations on the human arm with 22 human subjects. A pendulum with a variety of masses and contact bodies was used to exert impacts of increasing intensity until the load produced signs of bruising or swelling. We developed a statistical model from the maximum forces, peak pressures and maximum energy density measured, which enabled us to calculate injury limits for any percentile. The relative comparison of the injury limits for the 25th percentile with force and pressure pain limits for the 75th percentile confirmed that pain limits used in cobotics can prevent injuries on all the body locations tested, except body location (13) humerus.

Given the limited knowledge in the literature, we decided to test only four body locations on the human arm, the body part most frequently exposed to robot collisions. The number of body locations examined is much smaller than the 29 body locations for which pain limits exist (ISO/TS 15066, 2016). The limits for the human hand-arm system provide a starting point for future studies of injury onset limits for other body locations, though. Our findings and conclusions ought to be treated as preliminary since the subject groups tested were quite small. More data will have to be collected in other tests with more subjects. We intend to conduct a follow-up study with more subjects and under improved experimental conditions in the near future. MRI will replace visual examination in the envisioned follow-up study to eliminate false positive observations.

CRediT authorship contribution statement

R. Behrens: Writing – original draft, Software, Methodology, Data curation, Conceptualization. **G. Pliske:** Writing – review & editing, Conceptualization. **S. Piatek:** Writing – review & editing, Supervision, Methodology. **F. Walcher:** Supervision, Resources, Methodology. **N. Elkmann:** Writing – review & editing, Supervision, Resources, Project administration, Methodology.

Disclosure

This research was sponsored by the Mercedes-Benz Group and KUKA Roboter GmbH with the intention of evaluating the pain limits currently used in cobotics. None of the authors has any affiliation with either company nor any conflict of interest to disclose.

Declaration of competing interest

The authors declare that they have no known competing financial interests or personal relationships that could have appeared to influence the work reported in this paper.

Appendix

We used the following anatomical landmarks to localize the body locations:

(12) Deltoid m. The contact point lies in the lateral middle line of the upper arm. Its distance from the acromion is 50 mm.

(13) Humerus The contact point is on the line running from the acromion to the upper end of the elbow joint. Its cranial distance from the elbow joint is one-third of the line's length.

(15) Forearm m. The contact point lies a lateral distance of 40 mm from the supporting point, which is on the line running from the superior border's center to the outermost lateral point of the triquetral bone. The distance of the supporting point from the superior border's center is 100 mm.

(25) Back of the hand The contact point lies between the MCP (metacarpophalangeal joints) of the middle finger to the wrist. The distance from the MCP is one-third of the total distance from the MCP to the wrist.

References

Bader, D.L., Bowker, P., 1983. Mechanical characteristics of skin and underlying tissues in vivo. Biomaterials 4, 305–308. http://dx.doi.org/10.1016/0142-9612(83)90033-9.

Barington, K., Jensen, H.E., 2016. The impact of force on the timing of bruises evaluated in a porcine model. J. Forensic Leg. Med. 40, 61–66.

Behrens, R., Elkmann, N., 2014. Study on meaningful and verified thresholds for minimizing the consequences of human–robot collisions. In: 2014 IEEE International Conference on Robotics & Automation. ICRA, pp. 3378–3383. http://dx.doi.org/10.1109/ICRA.2014.6907345.

Behrens, R., Elkmann, N., 2021. A revised framework for managing the complexity of contact hazards in collaborative robotics. In: 2021 IEEE International Conference on Intelligence and Safety for Robotics. pp. 252–258. http://dx.doi.org/10.1109/ISR50024.2021.9419528.

Behrens, R., Pliske, G., Umbreit, M., Piatek, S., Walcher, F., Elkmann, N., 2022. A statistical model to determine biomechanical limits for physically safe interactions with collaborative robots. Front. Robotics AI 8, http://dx.doi.org/10.3389/frobt.2021.667818.

Bellamy, S.L., Li, Y., Ryan, L.M., Lipsitz, S., Canner, M.J., Wright, R., 2004. Analysis of clustered and interval censored data from a community-based study in asthma. Stat. Med. 23, 3607–3621. http://dx.doi.org/10.1002/sim.1918.

Black, H.I., Coupaud, S., Daéid, N.N., Riches, P.E., 2019. On the relationships between applied force, photography technique, and the quantification of bruise appearance. Forensic. Sci. Int. 305, 109998. http://dx.doi.org/10.1016/j.forsciint.2019.109998.

Cardany, C.R., Rodeheaver, G., Thacker, J., Edgerton, M.T., Edlich, R.F., 1976. The crush injury: A high risk wound. J. Am. College Emergency Physic. 5, 965–970. http://dx.doi.org/10.1016/S0361-1124(76)80123-2.

Cesari, D., Ramet, M., Clair, P.Y., 1980. Evaluation of pelvic fracture tolerance in side impact. In: 24th Stapp Car Crash Conference (1980), SAE International. http://dx.doi.org/10.4271/801306.

Crandall, J., Bose, D., Forman, J., Untaroiu, C., Arregui-Dalmases, C., Shaw, C., Kerrigan, J., 2011. Human surrogates for injury biomechanics research. Clinical Anatomy 24, 362–371. http://dx.doi.org/10.1002/ca.21152.

Delignette-Muller, M.L., Dutang, C., 2015. fitdistrplus: An r package for fitting distributions. J. Stat. Softw. 64, 1–34. http://dx.doi.org/10.18637/jss.v064.i04.

Delye, H., Verschueren, P., Depreitere, B., Verpoest, I., Berckmans, D., Vander, S.J., van der Perre, J., Goffin, G., 2007. Biomechanics of frontal skull fracture. J. Neurotrauma 24, 1576–1586. http://dx.doi.org/10.1089/neu.2007.0283.

Desmoulin, G.T., Anderson, G.S., 2011. Method to investigate contusion mechanics in living humans. J. Forensic Biomech. 2, 1–10. http://dx.doi.org/10.4172/2090-2697.1000107.

Dhaliwal, T.S., Beillas, P., Chou, C.C., Prasad, P., Yang, K.H., King, A.I., 2002. Structural response of lower leg muscles in compression: A low impact energy study employing volunteers, cadavers and the hybrid iii. Stapp Car Crash J. 46, 229–243.

Di Maio, V.J.M., Di Maio, D.J., 2001. Forensic pathology. In: CRC Series in Practical Aspects of Criminal and Forensic Investigations, second ed. CRC Press, Boca Raton.

Etheridge, B.S., Beason, D.P., Lopez, R.R., Alonso, J.E., McGwin, G., Eberhardt, A.W., 2005. Effects of trochanteric soft tissues and bone density on fracture of the female pelvis in experimental side impacts. Ann. Biomed. Eng. 33, 248–254. http://dx.doi.org/10.1007/s10439-005-8984-5.

Fujikawa, T., Sugiura, R., Nishikata, R., Nishimoto, T., 2017. Critical contact pressure and transferred energy for soft tissue injury by blunt impact in human–robot interaction. In: 2017 17th International Conference on Control, Automation and Systems. ICCAS, pp. 867–872. http://dx.doi.org/10.23919/ICCAS.2017.8204347.

Gadd, C.W., Nahum, A.M., Gatts, J., Danforth, J.P., 1968. A study of head and facial bone impact tolerances. In: Proceedings of the 9th Automotive Safety Seminar. pp. 1–8.

Hallowell, M.R., Alexander, D., Gambatese, J.A., 2017. Energy-based safety risk assessment: does magnitude and intensity of energy predict injury severity? Constr. Manag. Econ. 35, 64–77. http://dx.doi.org/10.1080/01446193.2016.1274418.

Han, D., Park, M.Y., Choi, J., Shin, H., Rhim, S., 2021. Analysis of human–robot physical interaction at collision. In: 2021 IEEE International Conference on Intelligence and Safety for Robotics. ISR, pp. 153–156. http://dx.doi.org/10.1109/ISR50024.2021.9419556.

Haut, R.C., 2002. Biomechanics of soft tissue. In: Nahum, A.M., Melvin, J.W. (Eds.), Accidental Injury. Springer New York, New York, NY, pp. 228–253. http://dx.doi.org/10.1007/978-0-387-21787-1_11.

Hentout, A., Aouache, M., Maoudj, A., Akli, I., 2019. Human–robot interaction in industrial collaborative robotics: a literature review of the decade 2008–2017. Adv. Robot. 33, 764–799. http://dx.doi.org/10.1080/01691864.2019.1636714.

Hodgson, V.R., Lange, W.A., Talwalker, R.K., 1965. Injury to the facial bones. SAE Technical Paper http://dx.doi.org/10.4271/650957.

Hodgson, V.R., Nakamura, G.S., Talwalker, R.K., 1964. Response of the facial structure to impact. SAE Technical Paper 22, 9–250.

ISO/TS 15066, 2016. Robots and Robotic Devices - Collaborative Robots. Technical Report, International Organization for Standardization.

J211-1, S., 2014. Instrumentation for Impact Test – Part 1 – Electronic Instrumentation. Technical Report, SAE International.

Kent, R.W., Funk, J.R., Kent, R.W., Funk, J.R., 2004. Data censoring and parametric distribution assignment in the development of injury risk functions from biochemical data \\ data censoring and parametric distribution assignment in the development of injury risk functions from biochemical data. SAE Technical Paper http://dx.doi.org/10.4271/2004-01-0317.

Kent, R., Patrie, J., 2005. Chest deflection tolerance to blunt anterior loading is sensitive to age but not load distribution. Forensic. Sci. Int. 149, 121–128. http://dx.doi.org/10.1016/j.forsciint.2004.04.086.

Kieser, J., Taylor, M., Carr, D.D., 2012. Forensic Biomechanics. Essentials of Forensic Science. Wiley-Blackwell, Chichester, West Sussex, UK.

King, A.I., Viano, D.C., Mizeres, N., States, J.D., 1995. Humanitarian benefits of cadaver research on injury prevention. J. Trauma 38 (4), 564–569, URL: http://worldcatlibraries.org/wcpa/oclc/173438501.

Krüger, J., Lien, T.K., Verl, A., 2009. Cooperation of human and machines in assembly lines. CIRP Ann. 58, 628–646. http://dx.doi.org/10.1016/j.cirp.2009.09.009.

Lacourt, T.E., Houtveen, J.H., van Doornen, L.J.P., 2012. Experimental pressure-pain assessments: Test-retest reliability, convergence and dimensionality. Scand. J. Pain 3, 31–37. http://dx.doi.org/10.1016/j.sjpain.2011.10.003.

Lindsey, J.C., Ryan, L.M., 1998. Methods for interval-censored data. Stat. Med. 17, 219–238. http://dx.doi.org/10.1002/(SICI)1097-0258(19980130)17:2<219::AID-SIM735>3.0.CO;2-O.

Mao, X., Yamada, Y., Akiyama, Y., Okamoto, S., Yoshida, K., 2015. Development of a novel test method for skin safety verification of physical assistant robots. In: Yu, H. (Ed.), 2015 IEEE International Conference on Rehabilitation Robotics. ICORR, IEEE, Piscataway, NJ, pp. 319–324. http://dx.doi.org/10.1109/ICORR.2015.7281219.

Melia, M., Geissler, B., König, J., Ottersbach, H.J., Umbreit, M., Letzel, S., Muttray, A., 2019. Pressure pain thresholds: Subject factors and the meaning of peak pressures. Eur. J. Pain 23, 167–182. http://dx.doi.org/10.1002/ejp.1298.

Mewes, D., Mauser, F., 2003. Safeguarding crushing points by limitation of forces. Int. J. Occupational Safety Ergonomics 9, 177–191. http://dx.doi.org/10.1080/10803548.2003.11076562.

Muggenthaler, H., Praxl, N., Adamec, J., Merten, K.v., Schönpflug, M., Graw, M., Schneider, K., 2006. The effects of muscle activity on human kinematics and muscle response characteristics – volunteer tests for the validation of active human models. SAE Technical Paper http://dx.doi.org/10.4271/2006-01-2370.

Nahum, A.M., Gadd, C.W., Schneider, D.C., Madeira, R.G., 1972. Tolerances of superficial soft tissues to injury. J. Trauma 12, 1044–1052.

Nyquist, G.W., 1986. Injury tolerance characteristics of the adult human lower extremities under static and dynamic loading. SAE Technical Paper http://dx.doi.org/10.4271/861925.

Park, M.Y., Han, D., Lim, J.H., Shin, M.K., Han, Y.R., Kim, D.H., Rhim, S., Kim, K.S., 2019. Assessment of pressure pain thresholds in collisions with collaborative robots. PLoS One 14, e0215890. http://dx.doi.org/10.1371/journal.pone.0215890.

Payne, T., Mitchell, S., Bibb, R., 2013. Design of human surrogates for the study of biomechanical injury: A review. Crit. Rev. Biomed. Eng. 41, 51–89. http://dx.doi.org/10.1615/CritRevBiomedEng.2013006847.

Pintar, F., Yoganandan, N., Eppinger, R.H., 1998a.. Response and tolerance of the human forearm to impact loading. In: SAE Technical Paper Series. SAE International400 Commonwealth Drive, Warrendale, PA, United States, http://dx.doi.org/10.4271/983149.

Pintar, F.A., Yoganandan, N., Voo, L., 1998b. Effect of age and loading rate on human cervical spine injury threshold. SPINE 23, 1957–1962. http://dx.doi.org/10.1097/00007632-199809150-00007.

Povse, B., Koritnik, D., Kamnik, R., Bajd, T., Munih, M., 2011. Emulation system for assessment of human–robot collision. Meccanica 46, 1363–1371. http://dx.doi.org/10.1007/s11012-010-9403-z.

Randeberg, L.L., Winnem, A.M., Langlois, N.E., Larsen, E.L., Haaverstad, R., Skallerud, B., Haugen, O.A., Svaasand, L.O., 2007. Skin changes following minor trauma. Lasers Surg. Med. 39, 403–413. http://dx.doi.org/10.1002/lsm.20494.

Raymond, D., van Ee, C., Crawford, G., Bir, C., 2009. Tolerance of the skull to blunt ballistic temporo-parietal impact. J. Biomech. 42, 2479–2485. http://dx.doi.org/10.1016/j.jbiomech.2009.07.018.

Saito, T., Ikeda, H., 2005. Measurement of human pain tolerance to mechanical stimulus of human-collaborative robots. Specific Res. Rep. Nat. Inst. Indust. Safety 33, 16–23.

Sharkey, E.J., Cassidy, M., Brady, J., Gilchrist, M.D., NicDaeid, N., 2012. Investigation of the force associated with the formation of lacerations and skull fractures. Int. J. Legal Med. 126, 835–844. http://dx.doi.org/10.1007/s00414-011-0608-z.

Shen, W., Niu, Y., Mattrey, R.F., Fournier, A., Corbeil, J., Kono, Y., Stuhmiller, J.H., 2008. Development and validation of subject-specific finite element models for blunt trauma study. J. Biomech. Eng. 130, 021022. http://dx.doi.org/10.1115/1.2898723.

Silver, F.H., Siperko, L.M., Seehra, G.P., 2003. Mechanobiology of force transduction in dermal tissue. Skin Res. Technol. 9, 3–23. http://dx.doi.org/10.1034/j.1600-0846.2003.00358x.

Smalls, L.K., Randall Wickett, R., Visscher, M.O., 2006. Effect of dermal thickness, tissue composition, and body site on skin biomechanical properties. Skin Res. Technol. 12, 43–49. http://dx.doi.org/10.1111/j.0909-725X.2006.00135x.

Stalnaker, R.L., Melvin, J.W., 1976. Human tolerance to lower extremities impacts. In: Proceedings of the 1976 IRCOBI Conference. pp. 362–374.

Sugiura, R., Fujikawa, T., Nishikata, R., Nishimoto, T., 2019. Soft tissue bruise injury by blunt impact in human–robot interaction - difference of tolerance between chest and extremities. In: 2019 19th International Conference on Control, Automation and Systems. ICCAS, IEEE, pp. 792–797. http://dx.doi.org/10.23919/ICCAS47443.2019.8971656.

Sun, J., 2006. The Statistical Analysis of Interval-Censored Failure Time Data, first ed. Springer, New York.

Szczesny, G., Veihelmann, A., Nolte, D., Messmer, K., 2001. Changes in the local blood and lymph microcirculation in response to direct mechanical trauma applied to leg: in vivo study in an animal model. J. Trauma 51, 508–517. http://dx.doi.org/10.1097/00005373-200109000-00014.

Viano, D.C., King, A.I., Melvin, J.W., Weber, K., 1989. Injury biomechanics research: An essential element in the prevention of trauma. J. Biomech. 22, 403–417. http://dx.doi.org/10.1016/0021-9290(89)90201-7.

Viano, D.C., Lau, I.V., 1988. A viscous tolerance criterion for soft tissue injury assessment. J. Biomech. 21, 387–399.

Villani, V., Pini, F., Leali, F., Secchi, C., 2018. Survey on human–robot collaboration in industrial settings: Safety, intuitive interfaces and applications. Mechatronics 55, 248–266. http://dx.doi.org/10.1016/j.mechatronics.2018.02.009.

Yamada, Y., Suita, K., Imai, K., Ikeda, H., Sugimoto, N., 1996. A failure-to-safety robot system for human–robot coexistence. Robot. Auton. Syst. 18, 283–291. http://dx.doi.org/10.1016/0921-8890(95)00075-5.

Zhou, Q., Rouhana, S.W., Melvin, J.W., 1996. Age effects on thoracic injury tolerance. In: SAE Technical Paper Series. SAE International400 Commonwealth Drive, Warrendale, PA, United States, http://dx.doi.org/10.4271/962421.